Intermixing during growth of InAs self-assembled quantum dots in InP: A photoluminescence and tight-binding investigation

C. Dion* and P. Desjardins
Regroupement Québécois sur les Matériaux de Pointe (RQMP), Département de génie physique, École Polytechnique de Montréal, Montréal, Québec, Canada H3C 3A7

N. Shtinkov
Department of Physics, University of Ottawa, Ottawa, Ontario, Canada K1N 6N5

M. D. Robertson
Department of Physics, Acadia University, Wolfville, Nova Scotia, Canada B4P 2R6

F. Schiettekatte
Regroupement Québécois sur les Matériaux de Pointe (RQMP), Département de physique, Université de Montréal, Montréal, Québec, Canada H3C 3J7

P. J. Poole and S. Raymond
Institute for Microstructural Sciences, National Research Council, Ottawa, Ontario, Canada K1A 0R6
(Received 20 September 2007; published 29 February 2008)

Atomic intermixing during the growth of self-assembled InAs quantum dots (QDs) in InP(001) by chemical beam epitaxy (CBE) can result in the formation of graded interfaces or even alloyed $InAs_{1-x}P_x$ QDs. Taking advantage of a series of samples in which photoluminescence (PL) spectra are characterized by the presence of a large number of distinct peaks corresponding to the emission from QD families having the same thicknesses (h_{QD}) in terms of an integer number of monolayers (MLs), we investigate intermixing by matching the experimentally observed transition energies to those calculated from tight-binding simulations. Two calculation frameworks are considered: (i) structures in which QDs are alloys with uniform P concentration [P] and (ii) nominally pure InAs QDs bordered by graded interfaces characterized by a diffusion length L_D. Excellent agreement between theory and experiment is achieved with either framework. The analysis reveals that the two frameworks yield similar composition profiles as the composition at the center of the QD in the case of graded interfaces is modified to a point where it becomes essentially equal to that calculated for a QD of uniform composition. The calculations also indicate that in both frameworks, two substantially different solution sets are compatible with the experimental results. The first one is characterized by all QDs having the same P composition independent of their size, while the second solution shows a decreasing degree of intermixing with increasing h_{QD}. To discriminate between the two solutions, we use them as input data in a Bloch-wave simulation of transmission electron microscopy (TEM) image contrast, providing a sequence of contrast versus h_{QD} values. Only the scheme in which the amount of [P] is the same for all QD ensembles is compatible with the TEM observations. From the analysis of an extensive array of CBE-deposited QD samples, it is concluded that the observed PL transitions can be attributed to a 3 ML thick wetting layer and 4–14 ML thick QDs, with [P] ranging from 6% to 10% depending on the growth conditions. The determined values of [P] and L_D suggest that surface As/P exchange and strain-driven alloying are the most probable mechanisms for substantial P incorporation.

DOI: 10.1103/PhysRevB.77.075338 PACS number(s): 78.67.Hc, 73.21.La, 68.37.Lp, 68.35.Fx

I. INTRODUCTION

The formation of atomically sharp interfaces in epitaxially grown heterojunctions is a difficult task since atomic intermixing between the different materials is often unavoidable due to the relatively high temperature used during deposition. This effect has been found to be particularly important during the growth of self-assembled quantum dots (QDs), and evidence of highly alloyed structures has been reported by several authors for a wide variety of semiconductor systems.[1–7] For instance, intermixing effects are significant in the InAs/InP system due to the rapid exchange of group-V atoms at interfaces[8–12] that can reach down to the two top monolayers (MLs).[13] This material system has been recognized for its promising applications in broadband[14] and single-photon[15] sources operating in the 1.5 μm wavelength range for optical communication networks. Because atomic intermixing modifies the confinement profile of the structure and alters the corresponding energy levels, it has a major impact on the QD emission characteristics and, consequently, on the properties of QD-based optoelectronic devices. Despite the importance of atomic intermixing in technological applications, assessing this effect in nanostructures remains very challenging, particularly for optically active QDs embedded in a matrix. For such structures, atomic intermixing can be analyzed via photoluminescence (PL) spectroscopy

since the optical transition energy is very sensitive to the material composition inside the confinement layer. However, analysis of atomic intermixing by optical techniques relies on theoretical calculations of the optical transition energies. Since a given transition energy is not unique to a particular structure with specific size and composition, the analysis of the PL spectra may become problematic. Complementary analyses are, thus, required for the unambiguous determination of the structural properties.

Atomic intermixing in the InAs/InP system has been investigated to some extent in quantum well (QW) structures. With the aid of PL, band structure calculations based on the envelope function approximation (EFA) for a square well model, and high-resolution x-ray diffraction data, a reasonable description of the optical emission from single QWs with thicknesses larger than 3 ML can be obtained.[16,17] However, in the case of QD samples where structures of various thicknesses are simultaneously present, these models could not provide a coherent description, using a single set of calculation parameters, of the experimentally observed transition energies as a function of the structure size. For example, major discrepancies between observed and calculated transition energies were obtained for QD structures less than 4 ML thick.[18–21] It was proposed by Carlin *et al.*[18] that such divergences originated from short-range interfacial roughness in the heterostructures, leading to the conclusion that QDs with fractional ML heights are present in the sample. However, Brasil *et al.*[22] have shown that this simple model failed to explain their results, indicating that the short-range roughness concept is inappropriate. By considering a 1 ML thick $InAs_{1-x}P_x$ interfacial layer on top of the InAs QDs, Folliot *et al.*[23] have suggested intermixing effects to explain the inconsistency between measured and modeled optical transition energies. Furthermore, assuming $InP/InAs_{1-x}P_x/InP$ structures with either uniform or graded P concentration profile in their tight-binding (TB) calculations, Shtinkov *et al.*[24] have demonstrated that intermixing effects are sufficient to explain the optical results. Nevertheless, these models were not confirmed using other characterization techniques for a self-consistent determination of the structural properties of an ensemble of QDs.

In the present work, we discuss a procedure that enables the unambiguous assignment of QD heights (h_{QD}) and composition to the observed PL transitions. It combines PL characterization and TB calculations as well as transmission electron microscopy (TEM) measurements and Bloch-wave (BW) simulations. PL is especially well suited for studying InAs/InP QDs since their spectra are characterized by distinct emission lines where each peak can be attributed to the ground state emission arising from a subset population of QDs which share the same thickness in terms of an integer number of monolayers.[25] In order to model the PL results, we have chosen the TB method over EFA due to its atomistic nature and accuracy in determining band structures in nanostructures of thickness less than 3 ML.[26] Since the current study aims to achieve a coherent description of layers down to a few MLs in thickness, it is not *a priori* obvious whether the model will have to take into account the details of the interface layers. Therefore, we have compared the measured transition energies to calculated values arising from two different P composition profiles: (i) $InP/InAs_{1-x}P_x/InP$ structures of uniform P concentration and abrupt interfaces, and (ii) $InP/InAs_{1-x}P_x/InP$ structures with a P diffusion concentration profile. In the end, both approaches lead to equally good descriptions of the PL spectra from as-grown material. However, both calculation strategies yield two solution sets compatible with experimental results. In order to determine which of the two solutions provides the best description of our as-grown QD samples, we have performed BW simulations of TEM diffraction contrast images. Only the solution set having a constant level of P incorporation in all QDs is compatible with both PL and TEM experimental results, therefore allowing a precise assignment of h_{QD} and P composition to the observed PL transitions.

II. EXPERIMENTAL PROCEDURES

The structures studied in this work were grown on exactly oriented (001) InP substrates by chemical beam epitaxy in a Riber 32P reactor from trimethylindium (TMIn), arsine (AsH_3), and phosphine (PH_3). AsH_3 and PH_3 were cracked at 850 °C in a fast switching high-temperature injector to produce predominantly As_2 and P_2. The growth parameters are specified in Table I for each sample. After desorption of the surface oxide, the growth was initiated with an InP buffer layer. Prior to the deposition of InAs, a growth interruption with an overpressure (t_P) of P_2 was used to smooth the surface and residual P_2 was pumped out of the growth chamber during an additional growth interruption (t_{vent}). Then, TMIn and As_2 were injected simultaneously into the chamber to grow the InAs layer. This was followed by a growth interruption time under an overpressure (t_{As}) of As_2 to allow the QDs to form. For some samples, the As_2 was purged from the chamber during t_{vent} before the growth of the next layer. In general, the InP capping layer was grown in two steps. The InP growth rate (R) was evaluated by growing InP/InAsP/InP superlattices followed by x-ray measurements. Because the growth rate of III-V semiconductors in chemical beam epitaxy is governed by the group-III element, the same growth rate can be assumed for the growth of InAs. Under this assumption, about 2.2 ML of InAs was deposited in all samples. Samples A–C were grown using a different InP capping rate, while samples D–F were grown with different interruption times and temperatures. The use of these different samples provided an extensive array of QDs to illustrate the variability in structure height and composition as a function of the growth conditions.

The as-grown InAs/InP QDs were characterized by low-temperature PL measurements. Measurements on samples A–C were carried out using the 632.8 nm line of a HeNe laser and acquired with a Bomem Fourier transform infrared spectrometer with thermoelectrically cooled InSb detector. Samples D–F were probed using the 532 nm line of a $Nd:YVO_4$ laser. Spectra were acquired using a CVI Digikrom 240 double grating spectrometer and a liquid-N_2-cooled Northcoast Scientific Ge detector. The energy resolution was about 4 meV for both acquisition systems. In all cases, the incident light power density was kept constant at 50 W cm^{-2}, with a beam spot of 50 μm in diameter. This

TABLE I. Sample description and growth parameters [time (t), growth rate (R), and temperature (T)].

	Sample A		Sample B		Sample C		Sample D		Sample E		Sample F	
Layers	t (s)	T (°C)	t (s)	T (°C)	t (s)	T (°C)	t (s)	T (°C)	t (s)	T (°C)	t (s)	T (°C)
t_{InP} $\left[\begin{matrix}R\\(\text{Å s}^{-1})\end{matrix}\right]$	900 [1.08]	515	900 [1.08]	515	900 [1.08]	515	900 [1.08]	510	900 [1.08]	495	750 [1.08]	515
t_P	10	515	10	515	10	515	10	510	10	495	10	515
t_{vent}	5	515	5	515	5	515	5	510	5	495	3	515
t_{InAs}	6	515	6	515	6	515	6	510	6	495	6	515
t_{As}	30	515	30	515	30	515	30	510	60	495	25	515
t_{vent}	5	515	5	515	5	515	5	510	0	495	0	515
$t_{InP}(1)$ $\left[\begin{matrix}R\\(\text{Å s}^{-1})\end{matrix}\right]$	120 [2.68]	515	120 [1.08]	515	120 [0.43]	515	600 [1.08]	510	600 [1.75]	495	300 [1.07]	515
$t_{InP}(2)$ $\left[\begin{matrix}R\\(\text{Å s}^{-1})\end{matrix}\right]$	300 [2.68]	515	300 [2.68]	515	300 [2.68]	515			306 [1.08]	495	2940 [2.68]	500

excitation power density proved to be sufficiently low to prevent any distortion of the spectra by an excess carrier population in the QDs.[25] In the following, we were successful in determining the structural properties of the QDs independent of the characterization conditions, which further demonstrated the strength of the analysis presented in this paper.

Structural investigation was performed on sample C by plan-view TEM imaging. The TEM specimens were prepared by low-angle polishing using an Allied High Tech Products, Inc. MultiPrep™ system without ion milling (see Refs. 27 and 28 for extensive details regarding the sample preparation). Diffraction contrast images were obtained using a Philips EM301 TEM operated at 100 kV. Bright-field diffraction contrast images were taken near the [111] zone-axis projection. This imaging condition was chosen since it produced the most pronounced visible contrast between the InAs QDs and the surrounding InP matrix.

III. PHOTOLUMINESCENCE CHARACTERIZATION

Figures 1(a) and 1(b) present the normalized PL emission spectra from samples A–F. All spectra are characterized by a broad QD emission band centered around 850 meV. In sample C, the low-intensity peak observed at 1160 meV can be attributed to the emission from the wetting layer (WL).[29] The slight differences in the overall peak positions, the relative intensities of the peaks, and the expression of the WL are consistent with those expected from the different growth conditions used.[29,30] For instance, the QDs in sample F had a shorter growth interruption time than in other samples, resulting in a lower QD density and, thus, in the appearance of a WL peak in the spectra.

Despite the different growth conditions, in all cases the QD emission band results from the superposition of up to ten inhomogeneously broadened peaks. These peaks arise from the fundamental electron–heavy-hole (e1-hh1) transitions of ensembles of QDs having the same thickness in terms of an integer number of ML.[25] Throughout this work, these ensembles are referred to as QD *families*. The discretization of the emission is due to the small aspect ratio of the InAs/InP QDs, implying that the emission energy is determined predominantly by the QD thickness. Typically, the QDs have a thickness ranging from 3 to 13 ML and a lateral dimension of 18–33 nm, leading to a height/diameter ratio of about 0.06.[28]

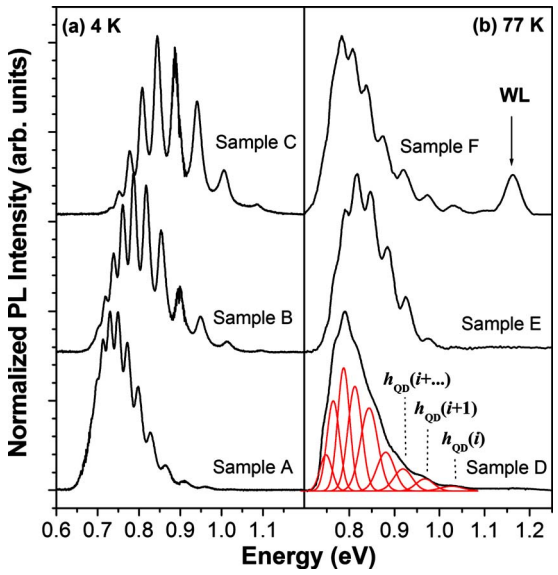

FIG. 1. (Color online) (a) Photoluminescence spectra from samples A–C. (b) Photoluminescence spectra from samples D–F. Each peak is labeled in terms of the height of the QD family (h_{QD}) in monolayers. A typical example of the peak fitting operation is illustrated for sample D.

If one evokes a particle-in-a-box analogy, the ground state energy of the particle is proportional to the sum of the inverse squares of each dimension. Therefore, the contribution of the lateral confinement to the ground state energies of electrons and holes, and hence to the transition energy, is small compared to that of the vertical confinement. We have obtained a more precise estimate of these contributions to the e1-hh1 transition energy using the method described in Ref. 31. For an 11 ML thick and 20 nm wide QD, the contribution to the e1-hh1 transition is ~700 meV for the vertical confinement energy versus ~26 meV for the lateral confinement energy. Moreover, Folliot *et al.*[23] have further argued that the lateral confinement energy in InAs/InP QDs is nearly cancelled by Coulomb binding. Based on these arguments, one can conclude that the emission energy of an InAs/InP QD is close to that of an InAs/InP QW of the same thickness, implying that the QD transition energies can be reasonably well described using models originally developed for QWs. This is in sharp contrast to InAs/GaAs QDs for which lateral confinement effects were found to be important because of the higher aspect ratios of such structures.[32,33] For example, Kim *et al.*[34,35] reported aspect ratios in the 0.21–0.37 range for InAs/GaAs QDs grown using different growth techniques.

The fundamental transition energy associated with each QD family was determined from the PL spectra using a multiparameter fit assuming a single Gaussian curve per emission peak. The full width at half maximum of the Gaussian peaks was constrained to increase with increasing emission energy, as variations in interface roughness cause larger relative changes to the confinement emission energy in thinner QDs.[23] Overall, this procedure allows the determination of the peak energy within ±5 meV uncertainty. A typical example of our fitting operation is illustrated for sample D in Fig. 1(b). In this figure, the peaks are labeled in terms of QD height (h_{QD}) with an incremental step of 1 ML. In the following, we determine the QD thickness by modeling the transition energies using TB calculations.

IV. ANALYSIS OF PHOTOLUMINESCENCE DATA USING TIGHT-BINDING CALCULATIONS

A. Description of the model and theoretical approach

As discussed in the previous section, the emission from our InAs/InP QDs is closely analogous to that from QWs so that their transition energies can be analyzed correspondingly. We have, thus, calculated the fundamental e1-hh1 transition energies in strained InAs/InP(001) QWs using the semi-empirical $sp^3d^5s^*$ nearest-neighbor TB model in the virtual crystal approximation and using the surface Green's function matching method. The details of the calculations, as well as a discussion of the TB parametrization, can be found in Ref. 24. The $sp^3d^5s^*$ model[36] was chosen over the commonly used sp^3s^* model because it provides a superior description of the band edge energies and effective masses for InAs and InP. The virtual crystal approximation was used for calculating the material parameters at the interfaces and in the $InAs_{1-x}P_x$ alloy. The surface Green's function matching formalism[37] was employed to obtain the local density of states providing the energies and the spatial distribution of the bound states. As usual in TB calculations, the heterojunction band offset was taken into account by adding a constant value to the diagonal TB parameters. The unstrained valence band offset (VBO) between InAs and InP used in our calculations was set to 0.35 eV. This value was deemed reasonable with respect to several results reported in the literature for the InAs/InP heterojunction.[24,38] The atomic layers were assumed to be coherently strained, and the distances between the atomic planes were calculated using macroscopic elasticity theory. A linear approximation for the bulk lattice constant and the elasticity moduli as a function of composition x in $InAs_{1-x}P_x$ was assumed. Finally, in order to allow a direct comparison between the experimental measurements recorded at 77 K and the calculations performed at 0 K, a correction of the Bose-Einstein type of −3.5 meV was applied to the calculated energy values.[39] From complementary analyses, this value corroborates with the observed redshift of energy peaks in the spectra taken at 77 K, which was found to be in the 2–6 meV range. On the other hand, as will be presented in Sec. VI B, an uncertainty of a few meV in the temperature correction is insignificant in the assignment of h_{QD} and P composition to the observed PL transitions.

The composition and size of self-assembled InAs/InP QDs may depend on various diffusion processes occurring during growth. In growth techniques using gases for the group-V elements, such as in chemical beam epitaxy, the P composition profile is first influenced by the rapid group-V exchange at the surface. During the switching of the gases for the deposition of the InAs or InP capping layers, As or P adatoms are rapidly desorbed and replaced by incoming P or As.[40] Earlier reports have suggested that the As/P exchange reaction can extend as far as 2 ML below the surface to create a diffusion concentration profile.[13] Next, the self-assembly of InAs QDs is achieved during a growth interruption under arsenic overpressure. During this time, the composite material formed by the buffer layer and the strained overlayer can relax its excess energy via a transition from two-dimensional to three-dimensional surface morphology (island formation) and/or via chemical exchange—the so-called strain-driven alloying effect.[41,42] In the case of InAs/InP, it was previously suggested that the chemical relaxation mode is non-negligible, which would uniformly alloy the structures.[43] Finally, during the deposition of a thick InP capping layer at high temperature, bulk atomic interdiffusion at the InAs/InP interfaces can also occur, thus further increasing the intermixing within the heterostructure.

Considering these multiple processes, atomic intermixing can take several forms, from interfacial intermixing to complete alloying of the InAs layer. In the present work, we have examined both possibilities by performing TB calculations for two types of input heterostructures, and in order to minimize the ambiguity between them, we introduce two different notations for the P concentration. The first intermixing framework considered assumes uniform alloying of the InAs structure, and, consequently, the system was modeled as $InP/InAs_{1-x}P_x/InP$ QWs with uniform P concentration [P] and abrupt interfaces. In our calculations, [P] was varied from 0 to 25%. The second calculation scheme assumed

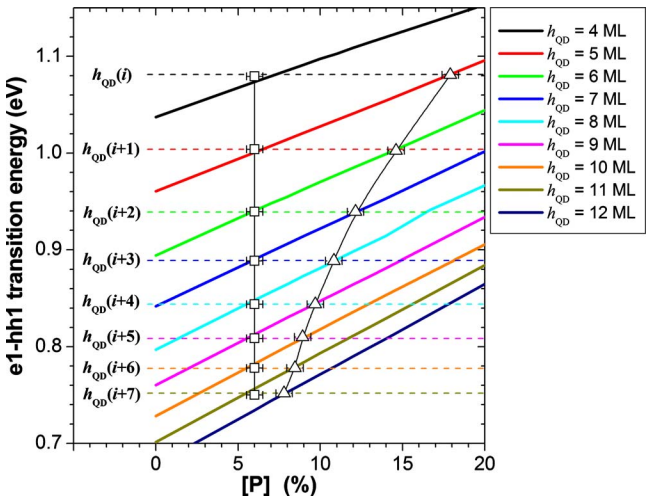

FIG. 2. (Color online) Calculated e1-hh1 transition energies for $InP/InAs_{1-x}P_x/InP$ QDs of different thicknesses as a function of the phosphorus concentration [P]. The dashed lines refer to the measured peak positions for sample C. The open squares and triangles illustrate the intersections between calculated and experimental transition energies corresponding to the two solution sets that describe the entire ensemble of QD families in a consistent manner.

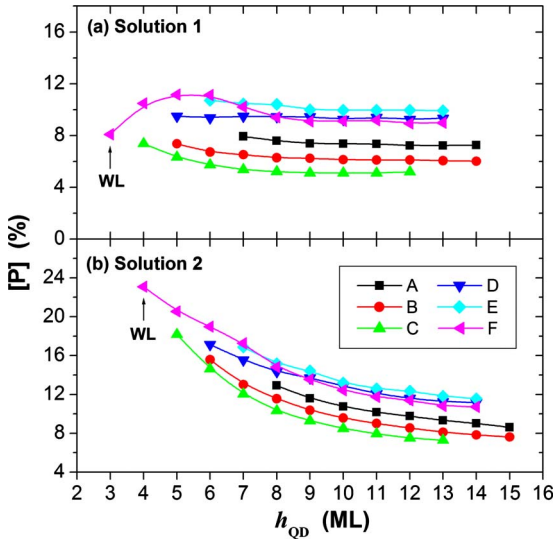

FIG. 3. (Color online) Phosphorus concentration [P] as a function of the QD height for samples A–F, as extracted from a comparison of the measured and the calculated transition energies.

symmetric interfacial intermixing effects, and the system was modeled using a P concentration profile (c_P) obtained from a Fickian diffusion model.[44] To determine the P concentration profile as a function of the position z and the time t during which the diffusion process occurs, the diffusion equations were analytically solved assuming a constant (i.e., time, strain, and concentration independent) diffusion coefficient D and an initial rectangular concentration profile. The solution is a superposition of error functions that depend on the diffusion length L_D and thickness according to[45]

$$c_P(z,t) = \frac{1}{2}\left[\mathrm{erfc}\left(\frac{z + h_{QD}/2}{L_D}\right) + \mathrm{erfc}\left(\frac{h_{QD}/2 - z}{L_D}\right)\right]. \quad (1)$$

In Eq. (1), L_D is a measure of the degree of interface grading and is defined as $L_D = \sqrt{4Dt}$.

B. Uniform phosphorous concentration: Results and comparison with experiments

Let us first consider the case where P is incorporated in the InAs QDs during growth in such a way that a uniform concentration [P] is obtained. The influence of the P concentration on the calculated e1-hh1 transition energy for $InP/InAs_{1-x}P_x/InP$ QDs is presented in bold lines in Fig. 2. It is observed that the transition energies of the QDs increase linearly with increasing [P]. For comparison with calculated results, the measured peak energies were traced with horizontal dashed lines and superimposed on the calculated transitions. From the intersections between the measured and calculated values, the QD height and P concentration were determined for each QD family in every QD sample. This procedure is illustrated in Fig. 2 using the optical transition energies from sample C. It can be seen that all measured peak positions agree with the calculated transition energies for nonzero [P] values. This clearly demonstrates the importance of considering intermixing to adequately describe the emission characteristics of self-assembled InAs/InP QDs, in excellent agreement with the findings of Refs. 23 and 24. In Fig. 2, one can further observe that each optical transition intercepts several of the calculated values corresponding to different QD heights, thus providing multiple solutions of (h_{QD}, [P]). However, we only consider solution sets of (h_{QD}, [P]) that logically describe the *ensemble* of QD emission lines, i.e., h_{QD} increasing by a step of 1 ML and [P] varying in a realistic manner, which excludes having negative values of [P]. Eliminating all unrealistic solution sets where [P] > 30%, only two possible solution sets remain. For illustration, the two solutions found for sample C are highlighted in Fig. 2 by open squares and triangles, respectively.

Figures 3(a) and 3(b) present the two solution sets of [P] as a function of the structure height for all samples under investigation. The first solution set attributes the emission to a 3 ML thick WL and QD families ranging from 4 to 14 ML in height, with [P] being relatively constant for all structures in a given sample. [P] is found to range from 6% to 10% depending on the growth conditions. For instance, it can clearly be seen for samples A–C that [P] increases with the InP capping rate. On the other hand, the solutions for samples D–F are nearly identical. One may note from the results for sample F that larger deviations from the mean value are observed for thinner QDs and WL thickness. This may be a result of the confinement energy in thinner structures being more sensitive to composition and strain variations.[23] For the second solution set, thicknesses of 4 ML and 5–15 ML are attributed to the WL and the QD families, respectively. In this case, a monotonically decreasing P content from about 23% to 8% as a function of h_{QD} is found.

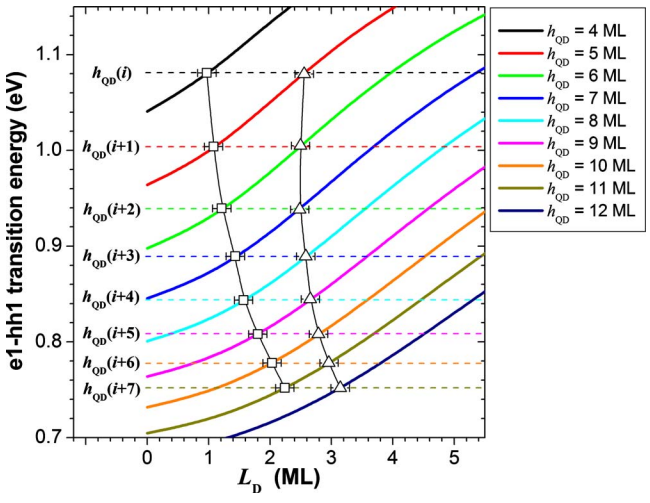

FIG. 4. (Color online) Calculated e1-hh1 transition energy for graded $InP/InAs_{1-x}P_x/InP$ QDs of different thicknesses as a function of L_D. The dashed lines refer to the measured peak positions for sample C, and the open squares and triangles correspond to two solution sets which consistently describe the entire ensemble of QD families.

In summary, a comparison between the PL measurements and TB calculations generated multiple solution sets of (h_{QD}, [P]). Among these, only two gave a consistent description of the entire ensemble of QD families, each of them possessing a distinct relationship between [P] and h_{QD}. Consequently, the consistent determination of QD physical parameters from PL characterization requires additional analysis in order to identify which solution set is the most physically realistic. We will address this point in Sec. V.

C. Graded interfaces: Results and comparison with experiment

As mentioned earlier, intermixing can also result in graded interfaces, which can be modeled by considering a P diffusion profile. Figure 4 displays in bold lines the calculated e1-hh1 transition energies for graded $InP/InAs_{1-x}P_x/InP$ QDs as a function of L_D, where $L_D=0$ relates to pure InAs QDs with abrupt interfaces and $L_D>0$ to QDs with graded interfaces. As expected, the transition energies of the graded QDs exhibit a blueshift with respect to energies associated with the undiffused rectangular QDs.[24] Fine dashed horizontal lines corresponding to the measured family peak positions are superimposed on the theoretical results to allow the identification of QD height and L_D for each QD family. Typical results of this procedure are presented in Fig. 4 using sample C as an example. As observed in the previous section, each measured optical transition energy corresponds to several calculated ones, thus supplying multiple solutions of (h_{QD},L_D). For the selection of realistic solution sets, we must again require that h_{QD} values increase in ML steps and that L_D is positive. This leads to two main solution sets of (h_{QD},L_D), which are highlighted for sample C with open symbols in Fig. 4.

The two solutions are presented in Fig. 5 for samples A–F.

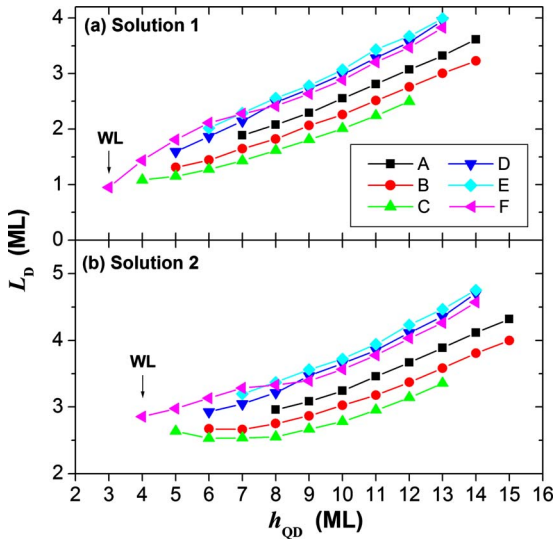

FIG. 5. (Color online) L_D as a function of the structure height for samples A–F, as extracted from a comparison of the measured and the calculated transition energies.

In the first and second solution sets, the WL and QD optical transitions are ascribed to thicknesses of 3 ML and 4–13 ML, and 4 ML and 5–14 ML, respectively. In both cases, L_D is seen to increase as a function of structure thickness, from 1 to 4 ML and from 2.5 to 4.5 ML in the first and second cases of QD family assignment, respectively. In order to obtain the P concentration incorporated within the InAs structures, Fig. 6 presents, as a function of h_{QD}, the P concentration at the center of the graded structure, $c_P(0,t)$, evaluated from the values of L_D determined in Fig. 5. In the first QD family assignment, $c_P(0,t)$ is found to be relatively constant for all structures of a given sample, while in the second case, $c_P(0,t)$ decreases monotonically with increasing h_{QD}.

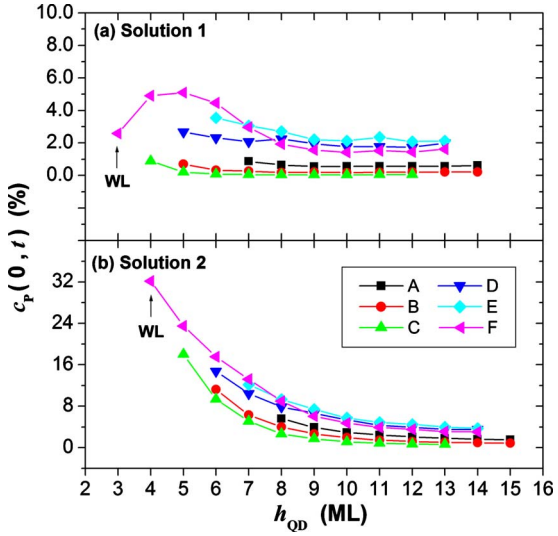

FIG. 6. (Color online) $c_P(0,t)$ as a function of the structure height for samples A–F, as extracted from a comparison of the measured and the calculated transition energies.

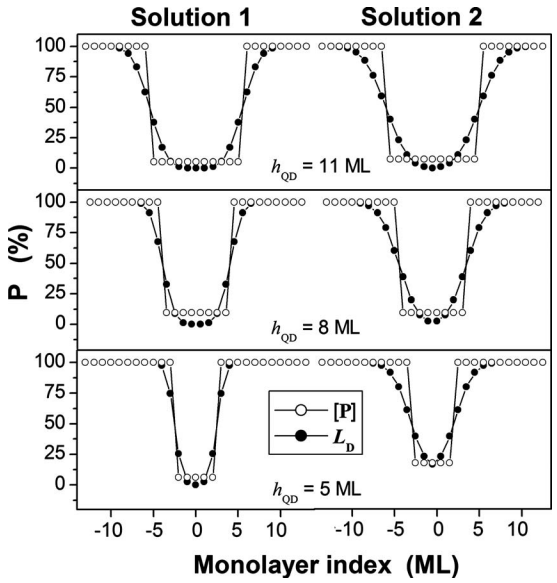

FIG. 7. P concentration profiles for various QD thicknesses in sample C evaluated from the solutions determined in the two calculation frameworks considered: (i) structures in which QDs are uniform alloys with P concentration [P] (open circles) and (ii) nominally pure InAs QDs bordered by graded interfaces characterized by a diffusion length L_D (filled circle). As shown in Figs. 3 and 6, the first solution set is characterized by QDs having the same P composition independent of their size, while the second one shows a decreasing degree of intermixing with increasing h_{QD}.

D. Comparison between the two calculation frameworks

Despite differing physical assumptions, calculation frameworks using either $InP/InAs_{1-x}P_x/InP$ with uniform P concentration or graded interfaces were found to be equally good in their description of the optical emission characteristics of InAs/InP QDs. Indeed, as shown in the two previous sections, both calculation frameworks lead to two consistent solution sets of (h_{QD}, [P] or $c_P(0,t)$), where the first set revealed 3–13 ML thick structures with fixed P composition, and the second set had 4–14 ML high structures with decreasing P composition. To further highlight the similarities between the two intermixing frameworks, Fig. 7 compares the P concentration profile determined from the two solution sets of (h_{QD}, [P]) and (h_{QD}, L_D) in sample C for various QD thicknesses. Figure 7 convincingly shows that a uniform square profile provides a reasonable approximation of the P diffusion profile for all QD sizes for both solutions. Actually, to achieve the confinement profile required to match the experimentally observed optical transitions, the interdiffusion at the interfaces must be so extensive that the composition at the center of the QD becomes significantly modified. In this context, differences between the two frameworks become less significant. This is undoubtedly an important conclusion since one could choose a particular solution over the other to simplify calculations for further growth and postgrowth intermixing studies.

Considering the above discussion, we now focus on determining which one of the two solutions (constant vs decreasing P content with increasing h_{QD}) provides the best description of our as-grown QD samples. This can be achieved by cross-referencing these solutions with structural analysis of the QDs using TEM imaging and BW simulations. Because Fig. 7 shows that the P concentration profiles are similar in the two frameworks, such small differences in P content are not likely to be quantifiable in TEM, and we complete our investigation by considering only QD structures with a uniform [P] profile.

V. TRANSMISSION ELECTRON MICROSCOPY INVESTIGATION

In the previous section, the comparison between optical and calculated transition energies yielded two reasonable solution sets of (h_{QD}: [P]), one where [P] is relatively constant for all structures in a given sample and another for which [P] significantly decreases with increasing structure thickness. In this section, we exploit TEM investigations and BW simulations to determine which of these two solutions provides the best description of our as-grown QD samples. However, as for the case of PL simulations, the solutions determined from the correspondence between experimental and simulated TEM images are not unique. Fortunately, we are able to show that the combination of PL and TEM allows the unambiguous assignment of QD height and composition. In this regard, we make use of sample C, which was the subject of a previous TEM characterization by Robertson *et al.*[28] A typical plan-view TEM image of this sample is shown in Fig. 8(a). Line scans across the long axis of the observed QDs were performed to determine the experimental contrast ratios, defined as the difference in intensity between the background (I_B) and the minimum intensity of the QD (I_{QD}) normalized to the intensity of the background.[28] Examples of line scan across observed QDs are presented in Fig. 8(b). Data were collected for about 400 QDs from two different regions on the sample. A probability histogram of the experimental contrast revealed seven distinct populations of QDs, in agreement with the number of QD families observed in PL spectra. The mean contrast value and standard deviation for each ensemble are shown with white bars in Fig. 9(b).

From the PL-TB analysis presented, the two possible solution sets obtained for sample C are explicitly (1) WL and QDs with thicknesses of 3 ML and 4–10 ML, respectively, with [P]=6%; and (2) WL and QDs with thicknesses of 4 ML and 5–11 ML, respectively, with [P] varying from 23% to 8.5%. Figure 9(a) shows schematically these two solutions, where darker shades of gray correspond to larger P concentrations. These solutions were used as input data for the simulation of contrast in the TEM image based on the approach presented in Ref. 28. The simulations were realized by modeling the elastic strain field using a finite-element method[46] that incorporates the effects of strain on the elastic constants of the QD,[47] and by modeling the TEM contrast using the many-beam BW method.[48] These simulations were used to generate a sequence of contrast ratios as a function of h_{QD} that was compared with experimental observations. The resulting sequences of theoretical and experimental contrast ratios are shown in Fig. 9(b). It can be seen that the contrast ratios computed using the first solution set, in which there is

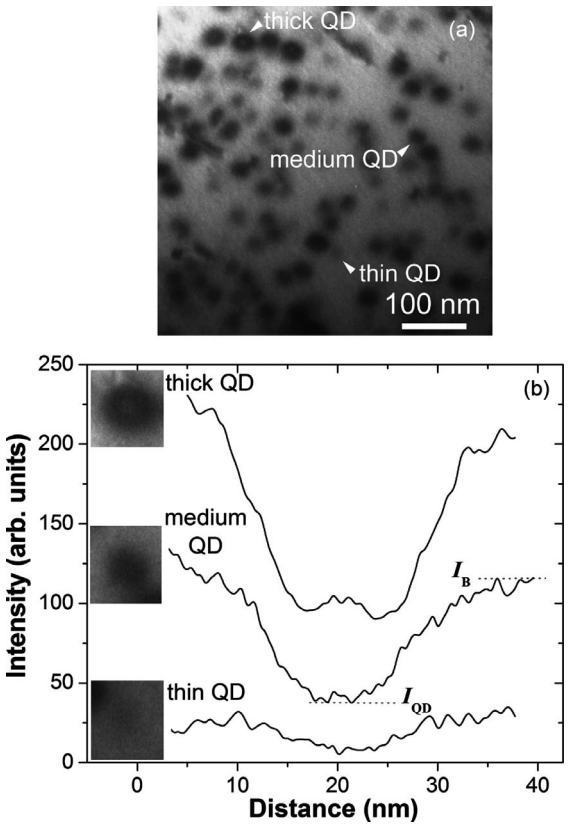

FIG. 8. (a) A plan-view, diffraction-contrast image of sample C near the [111] zone-axis orientation revealing the embedded QDs. The specimen increases in thickness from the top to the bottom of the image. (b) Examples of line scan profiles across observed QDs of different thicknesses. The lines from thick and thin QDs have been intentionally offset by 50 units for ease of visualization.

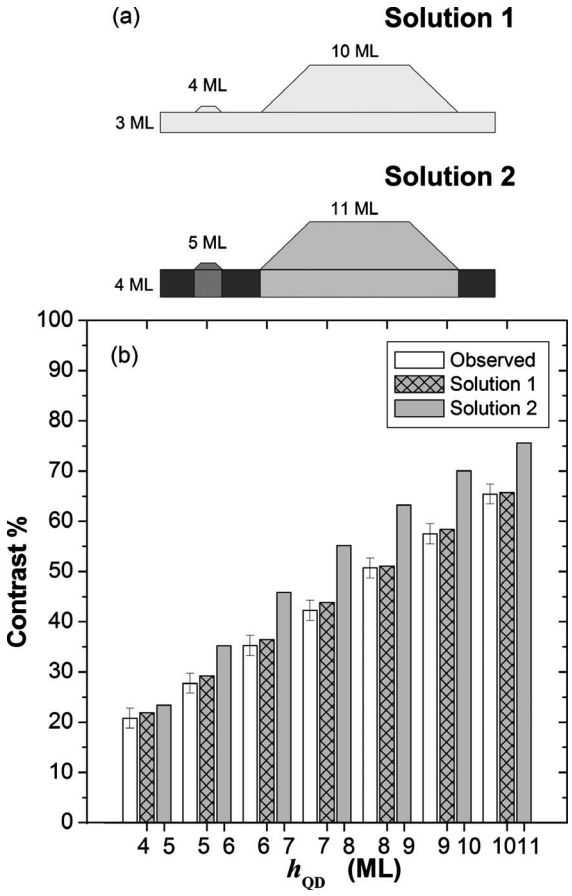

FIG. 9. (a) Schematic representation of the geometry of the InAs/InP QD system as implied by the two possible solutions obtained from analyzing PL and TB results of sample C. QDs that belong to the first and the last of the observed QD families are shown. Darker shades of gray correspond to larger P concentrations. (b) Comparison between the observed image contrast (white bars) with those predicted for (solution 1, gray bars and sparse pattern) WL and QDs of 3 ML and 4–10 ML with [P]=6%, and (solution 2, gray bars) WL and QDs of 4 ML and 5–11 ML with [P] varying from 23% to 8.5%.

a fixed P composition of 6% for all QD families, accurately reproduce the experimentally observed results. Additional simulations varying [P] allowed us to estimate an error of $\pm 2.6\%$ on [P] determined via combined TEM and BW characterization. In contrast to the latter results, the simulated contrast ratios obtained using the second solution set describing QDs with decreasing P composition clearly lie outside the 95% confidence intervals of the experimental results. We, thus, conclude that the scheme in which the degree of intermixing is the same for all QD families in a given sample provides a more realistic description of as-grown InAs/InP QDs. Thus, the QD height and P composition have been uniquely determined by using a combination of PL and TEM characterization, and the results indicate that P incorporation in the nominally pure InAs QDs is necessary to obtain a description of the sample which is compatible with all experimental data.

VI. DISCUSSION

A. Intermixing mechanism

As stated in Sec. IV A, several mechanisms could lead to a significant P incorporation into InAs structures during epitaxial growth, namely, bulk interdiffusion,[49] surface As/P exchange,[40] and strain-driven alloying.[43] Concerning bulk interdiffusion, Sallese *et al.*[49] have used PL combined with envelope function calculations to study interdiffusion in InAs/InP QDs submitted to postgrowth thermal annealing. Assuming that interdiffusion is a thermally activated process, i.e., $D=D_0 \exp(-E_a/k_BT)$, where E_a is the activation energy, D_0 is the pre-exponential factor, and k_B is the Boltzmann constant, the authors have found $D_0=16\ \mathrm{cm}^2\ \mathrm{s}^{-1}$ and $E_a=3.8\pm0.2$ eV. Based on this work, we can estimate the corresponding L_D for bulk interdiffusion during growth of the InP capping layer in our samples. For the growth of an InP capping layer at 500 °C for 1 h, we estimate a diffusion length of $L_D \sim 0.016$ ML. This value is 1 order of magnitude lower than those presented in Fig. 4, thereby indicating that bulk interdiffusion cannot be the main physical process for significant P incorporation into the QDs.

A second mechanism leading to P incorporation is surface As/P exchange. Using x-ray photoelectron spectroscopy,

TABLE II. QD family assignment and [P] as determined using our approach from PL characteristics of Refs. 21, 23, and 49–51. In our calculations, the VBO was set to 0.35 eV.

	Reported	This work	
Authors	h_{QD} (ML)	h_{QD} (ML)	[P] (%)
Gustafsson *et al.*[a]	2–8	3–9	9 ± 4
Folliot *et al.*[b]	4–8	6–10	10 ± 1
Sallese *et al.*[c]	2–11	3–12	11 ± 2
Michon *et al.*[d]	4–10	5–11	11 ± 2
Sakuma *et al.*[e]	3–10	4–11	6.1 ± 0.6
This work	5–13	5–13	9.6 ± 0.7

[a]Reference 21.
[b]Reference 23.
[c]Reference 49.
[d]Reference 50.
[e]Reference 51.

Law *et al.*[40] have characterized the initial stages of InAs/InP heterojunction formation through surface As/P exchange. They have determined the D_0 and E_a values for As diffusion into InP to be $(2.3 \pm 1.0) \times 10^{-7}$ cm^2 s^{-1} and (1.7 ± 0.2) eV, respectively. Assuming similar values for P diffusion into InAs and considering that surface As/P exchange occurs during the gas purge and InAs deposition steps, i.e., for a total time of ~15 s, we estimate $L_D \sim 1.0$ ML. This latter value is of the same order as those obtained in Fig. 4, suggesting that As/P exchange is a potential candidate to explain P incorporation.

Strain-driven alloying of the InAs layer during self-assembly could be another important source of P incorporation. Indeed, Brault *et al.*[43] have suggested that the chemical relaxation mode is non-negligible in the InAs/InP system since the positive enthalpy of mixing ΔH_m is small enough, so the system can relax part of its total energy by producing an interfacial alloy between the overlayer and the buffer layer prior to any change of the growth mode. Although not quantifiable due to lack of data in the literature, strain-driven alloying could also play a significant role in P incorporation in InAs structures in addition to As/P exchange.

The above discussion suggests that P incorporation in InAs strained layers could be a phenomenon common to all InAs growth methods involving the presence of phosphorous in the growth environment during InAs deposition. It is, therefore, of interest to extend our investigation to the analysis of PL spectra reported by other authors.[21,23,49–51] Using the PL-TB combination approach and assuming a constant [P] within the ensemble of QDs, we have determined the QD height and [P] composition related to the reported PL spectra and these results are presented in Table II.

The optical transition energies for each sample can be reproduced by our model of P incorporation, where the QD ensembles are characterized by [P] varying between 6% and 11%. Our analysis also leads to QD height assignments somewhat higher than previously reported. The slight variation in P content from sample to sample, in the same range as for the samples presented in this paper, can probably be attributed to the variability in the specific growth conditions used for each experiment. As for the QD height, most of the QD family assignments reported by these authors were based on the pioneering work of Gustafsson *et al.*[21] and Carlin *et al.*,[18] in which the family attribution was achieved through theoretical calculations of the transition energy via EFA. However, Carlin *et al.*[18] did not consider P incorporation in their model. By doing so, our approach suggests an alternative QD family assignment shifted by either 1 or 2 ML. This work, thus, demonstrates that fast and precise characterization of the initial state of as-grown InAs/InP QD ensembles for a wide variety of samples can be obtained from matching simple PL measurements and band structure calculations. The solutions obtained in this way are also in agreement with TEM analysis.

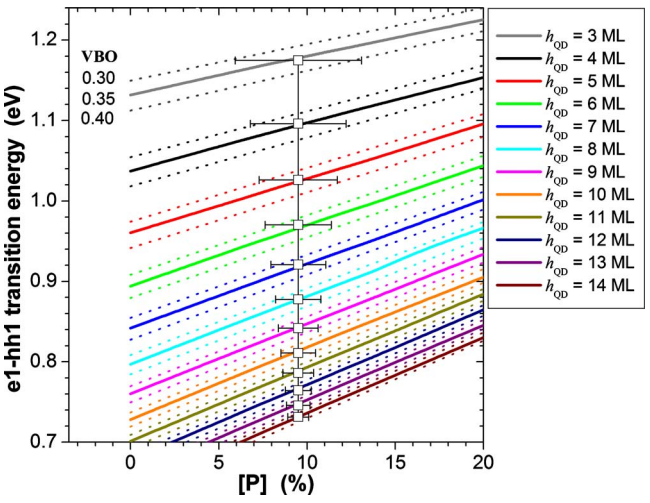

FIG. 10. (Color online) Calculated e1-hh1 transition energy for InP/InAs$_{1-x}$P$_x$/InP QDs of different thicknesses as a function of [P] and for values of the InAs/InP VBO of 0.30, 0.35, and 0.40 eV. The error bars show the uncertainty associated with the VBO in the determination of [P] from the optical transition energy.

B. Uncertainties on h_{QD} and [P]

Several factors could result in errors in the QD heights and P compositions as determined from the combination of measured PL characteristics and TB calculations. The first factor is that the InAs/InP VBO is not precisely known, with the values quoted in the literature ranging from 0.3 to 0.4 eV.[38] In order to determine the error associated with the uncertainty in the value for the VBO, the analysis in Sec. IV B was repeated for values from 0.3 to 0.4 eV. Figure 10 presents the calculated e1-hh1 transition energy for InP/InAs$_{1-x}$P$_x$/InP QDs as a function of [P], where the junctions between the experimental and theoretical transition energies are highlighted with open squares for a VBO of 0.35 eV. Error bars are added to these points in order to encompass the calculated transition energies for a VBO ranging from 0.30 to 0.40 eV. It can be seen that the uncertainty due to the VBO does not alter the h_{QD} values attributed to the optical transitions, but induces a noticeable uncertainty in [P]

values. The error on [P] decreases as a function of the structure thickness, decreasing from $\pm 4\%$ to 0.7% as h_{QD} increases from 3 to 14 ML. Another source of uncertainty is strain relaxation occurring during the QD formation, which leads to a reduction of strain in the InAs QDs compared to that expected for a uniform-thickness InAs QW layer (3.1%).[52] However, previous results have shown that the dependence of the e1-hh1 transition energy on strain is relatively weak for thin QWs.[24] For example, for a 4 ML thick QW, a reduction of the strain down to 2.5% lowers the transition energy by only 5 meV, resulting in an underestimation of the P concentration by at most 1%. In comparison, the experimental error on the energy of the optical transitions, ± 5 meV, leads to an error on [P] of $\pm 0.6\%$. This indicates that the main source of uncertainty on the P concentrations determined using the above procedure is due to an imprecise knowledge of the VBO.

VII. CONCLUSION

In this work, we have determined the height and composition of self-assembled InAs/InP QDs by combining PL and TEM measurements with TB and BW simulations. The TB calculations were performed assuming $InP/InAs_{1-x}P_x/InP$ QDs with either uniform P concentration with abrupt interfaces or a diffused P concentration profile. Both calculation frameworks were found to be equivalent in determining two possible solution sets of QD height and P composition, whereas the P concentration is either fixed or decreasing as a function of structure thickness. By cross-referencing these solutions with TEM analyses, it was found that the scheme in which the P concentration is fixed across all structures provided the most realistic description of as-grown InAs/InP QDs. Quantitatively, this implies that nominally pure InAs QDs have a P concentration of the order of 6%–10%, which could be explained by a combination of As/P exchange and strain-driven alloying. Therefore, by assuming a constant P concentration in all QDs of the same sample, one can determine the as-grown state of a sample from a simple PL experiment combined with TB calculations. This work, thus, provides a baseline for further growth and postgrowth intermixing studies.

ACKNOWLEDGMENTS

The authors acknowledge the National Science and Engineering Research Council of Canada, the National Research Council of Canada, and the Canada Research Chair program for financial support. The authors also acknowledge Goef Aers for insightful discussions and Jacques Lefebvre for its implication in PL measurements.

*Corresponding author. Also at the Institute for Microstructural Sciences, National Research Council, Ottawa, Ontario, Canada K1A 0R6.

[1] Y. Tu and J. Tersoff, Phys. Rev. Lett. **98**, 096103 (2007).
[2] P. D. Quinn, N. R. Wilson, S. A. Hatfield, C. F. McConville, G. R. Bell, T. C. Q. Noakes, P. Bailey, S. Al-Harthi, and F. Gard, Appl. Phys. Lett. **87**, 153110 (2005).
[3] A. Lemaitre, G. Patriarche, and F. Glas, Appl. Phys. Lett. **85**, 3717 (2004).
[4] M. Sztucki, T. U. Schulli, T. H. Metzger, E. Beham, D. Schuh, and V. Chamard, Superlattices Microstruct. **36**, 11 (2004).
[5] U. Denker, M. Stoffel, and O. G. Schmidt, Phys. Rev. Lett. **90**, 196102 (2003).
[6] P. M. Koenraad, D. M. Bruls, J. H. Davies, S. P. A. Gill, Fei Long, M. Hopkinson, M. Skolnick, and J. H. Wolter, Physica E (Amsterdam) **17**, 526 (2003).
[7] I. Kegel, T. H. Metzger, A. Lorke, J. Peisl, J. Stangl, G. Bauer, J. M. Garcia, and P. M. Petroff, Phys. Rev. Lett. **85**, 1694 (2000).
[8] Benzhong Wang, Fanghai Zhao, Yuheng Peng, Zhi Jin, Yudong Li, and Shiyong Liu, Appl. Phys. Lett. **72**, 2433 (1998).
[9] N. Carlsson, T. Junno, L. Montelius, M.-E. Pistol, L. Samuelson, and W. Seifert, J. Cryst. Growth **191**, 347 (1998).
[10] Y. Moon and E. Yoon, J. Cryst. Growth **212**, 61 (2000).
[11] N. Kobayashi and Y. Kobayashi, J. Cryst. Growth **124**, 525 (1992).
[12] L. G. Quagliano, B. Jusserand, and D. Orani, Phys. Rev. B **56**, 4919 (1997).
[13] J. M. Moison, M. Bensoussan, and F. Houzay, Phys. Rev. B **34**, 2018 (1986).
[14] F. Delorme, IEEE J. Quantum Electron. **34**, 1706 (1998).
[15] S. Frederick, D. Dalacu, D. Poitras, G. C. Aers, P. J. Poole, J. Lefebvre, D. Chithrani, and R. L. Williams, Microelectron. J. **36**, 197 (2005).
[16] P. Paki, R. Leonelli, L. Isnard, and R. A. Masut, J. Vac. Sci. Technol. A **18**, 956 (2000).
[17] R. Leonelli, C. A. Tran, J. L. Brebner, J. T. Graham, R. Tabti, R. A. Masut, and S. Charbonneau, Phys. Rev. B **48**, 11135 (1993).
[18] J. F. Carlin, R. Houdre, A. Rudra, and M. Ilegems, Appl. Phys. Lett. **59**, 3018 (1991).
[19] R. P. Schneider, Jr. and B. W. Wessels, J. Appl. Phys. **70**, 405 (1991).
[20] A. Bitz, C. Jordan, M. Di Ventra, K. A. Mader, L. C. Andreani, J. F. Carlin, A. Rudra, and J. L. Staehli, Nuovo Cimento Soc. Ital. Fis., D **17**, 1367 (1995).
[21] A. Gustafsson, D. Hessman, L. Samuelson, J. F. Carlin, R. Houdre, and A. Rudra, J. Cryst. Growth **147**, 27 (1995).
[22] M. J. S. P. Brasil, R. E. Nahory, M. C. Tamargo, and S. A. Schwarz, Appl. Phys. Lett. **63**, 2688 (1993).
[23] H. Folliot, S. Loualiche, B. Lambert, V. Drouot, and A. LeCorre, Phys. Rev. B **58**, 10700 (1998).
[24] N. Shtinkov, P. Desjardins, and R. A. Masut, Phys. Rev. B **66**, 195303 (2002).
[25] S. Raymond, S. Studenikin, S.-J. Cheng, M. Pioro-Ladriere, M. Ciorga, P. J. Poole, and M. D. Robertson, Semicond. Sci. Technol. **18**, 385 (2003).
[26] A. Di Carlo, Semicond. Sci. Technol. **18**, 1 (2003).
[27] M. D. Robertson, M. Burns, and T. Morrison, Microscopical Society of Canada Bulletin **33**, 19 (2006).

[28] M. D. Robertson, J. C. Bennett, A. M. Webb, J. M. Corbett, S. Raymond, and P. J. Poole, Ultramicroscopy **103**, 205 (2005).
[29] P. J. Poole, J. McCaffrey, R. L. Williams, J. Lefebvre, and D. Chithrani, J. Vac. Sci. Technol. B **19**, 1467 (2001).
[30] P. J. Poole, R. L. Williams, J. Lefebvre, and S. Moisa, J. Cryst. Growth **257**, 89 (2003).
[31] N. Shtinkov, P. Desjardins, R. A. Masut, and S. J. Vlaev, Phys. Rev. B **70**, 155302 (2004).
[32] R. Heitz, F. Guffarth, K. Potschke, A. Schliwa, D. Bimberg, N. D. Zakharov, and P. Werner, Phys. Rev. B **71**, 045325 (2005).
[33] U. W. Pohl, K. Potschke, A. Schliwa, F. Guffarth, D. Bimberg, N. D. Zakharov, P. Werner, M. B. Lifshits, V. A. Shchukin, and D. E. Jesson, Phys. Rev. B **72**, 245332 (2005).
[34] Jin Soo Kim, Jin Hong Lee, Sung Ui Hong, Won Seok Han, Ho-Sang Kwack, and Dae Kon Oh, J. Cryst. Growth **255**, 57 (2003).
[35] Sung Ui Hong, Jin Soo Kim, Jin Hong Lee, Ho-Sang Kwack, Won Seok Han, and Dae Kon Oh, J. Cryst. Growth **260**, 343 (2004).
[36] J.-M. Jancu, R. Scholz, F. Beltram, and F. Bassani, Phys. Rev. B **57**, 6493 (1998).
[37] F. Garcia-Moliner and V. R. Velasco, *Theory of Single and Multiple Interfaces* (World Scientific, Singapore, 1992).
[38] I. Vurgaftman, J. R. Meyer, and L. R. Ram-Mohan, J. Appl. Phys. **89**, 5815 (2001).
[39] L. Malikova, F. H. Pollak, R. A. Masut, P. Desjardins, and L. G. Mourokh, J. Appl. Phys. **94**, 4995 (2003).
[40] D. C. Law, Y. Sun, C. H. Li, S. B. Visbeck, G. Chen, and R. F. Hicks, Phys. Rev. B **66**, 045314 (2002).
[41] J. Tersoff, Phys. Rev. Lett. **74**, 434 (1995).
[42] D. J. Tweet, H. Matsuhata, R. Shioda, H. Oyanagi, and H. Kamei, Appl. Phys. Lett. **67**, 1286 (1995).
[43] J. Brault, M. Gendry, G. Grenet, G. Hollinger, Y. Desieres, and T. Benyattou, Appl. Phys. Lett. **73**, 2932 (1998).
[44] N. Shtinkov, V. Donchev, K. Germanova, and H. Kolev, Semicond. Sci. Technol. **15**, 946 (2000).
[45] R. W. Balluffi, S. M. Allen, and W. C. Carter, *Kinetics of Materials* (Wiley-Interscience, New York, 2005).
[46] D. Bimberg, M. Grundmann, and N. N. Ledenstov, *Quantum Dot Heterostructures* (Wiley, New York, 1999).
[47] S. W. Ellaway and D. A. Faux, J. Appl. Phys. **92**, 3027 (2002).
[48] C. J. Humphreys, Rep. Prog. Phys. **42**, 1825 (1979).
[49] J. M. Sallese, S. Taylor, H. J. Buhlmann, J. F. Carlin, A. Rudra, R. Houdre, and M. Ilegems, Appl. Phys. Lett. **65**, 341 (1994).
[50] A. Michon, I. Sagnes, G. Patriarche, G. Beaudoin, M. N. Merat-Combes, and G. Saint-Girons, J. Appl. Phys. **100**, 033508 (2006).
[51] Y. Sakuma, M. Takeguchi, K. Takemoto, S. Hirose, T. Usuki, and N. Yokoyama, J. Vac. Sci. Technol. B **23**, 1741 (2005).
[52] M. Grundmann, O. Stier, and D. Bimberg, Phys. Rev. B **52**, 11969 (1995).